RSC Advances

PAPER

View Article Online
View Journal | View Issue

Cite this: *RSC Adv.*, 2021, **11**, 7610

A rapid "on–off–on" mitochondria-targeted phosphorescent probe for selective and consecutive detection of Cu^{2+} and cysteine in live cells and zebrafish†

Peipei Deng,‡[a] Yongyan Pei,‡[a] Mengling Liu,[a] Wenzhu Song,[a] Mengru Wang,[a] Feng Wang,*[b] Chunxian Wu[a] and Li Xu*[a]

Received 23rd December 2020
Accepted 9th February 2021

DOI: 10.1039/d0ra10794h

rsc.li/rsc-advances

The detection of mitochondrial Cu^{2+} and cysteine is very important for investigating cellular functions or dysfunctions. In this study, we designed a novel cyclometalated iridium(III) luminescence chemosensor Ir bearing a bidentate chelating pyrazolyl-pyridine ligand as a copper-specific receptor. The biocompatible and photostable Ir complex exhibited not only mitochondria-targeting properties but also an "on–off–on" type phosphorescence change for the reversible dual detection of Cu^{2+} and cysteine. Ir had a highly sensitive (detection limit = 20 nM) and selective sensor performance for Cu^{2+} in aqueous solution due to the formation of a non-phosphorescent Ir–Cu(II) ensemble through 1 : 1 binding. According to the displacement approach, Ir was released from the Ir–Cu(II) ensemble accompanied with "turn-on" phosphorescence in the presence of 0–10 μM cysteine, with a low detection limit of 54 nM. This "on–off–on" process could be accomplished within 30 s and repeated at least five times without significant loss of signal strength. Moreover, benefiting from its good permeability, low cytotoxicity, high efficiency, and anti-interference properties, Ir was found to be suitable for imaging and detecting mitochondrial Cu^{2+} and cysteine in living cells and zebrafish.

1 Introduction

The development of new synthetic luminescence probes for the efficient recognition and sensing of biologically relevant cations and amino acids has received considerable interest because of their important roles in chemistry, environmental science, and biology over the past few years.[1–5] In particular, Cu^{2+} is a ubiquitous metal element present in the human body that plays vital roles in regulating many biological processes.[6] However, excessive concentration of Cu^{2+} in the body can result in oxidative damage to some important biomolecules, including proteins, nucleic acids and lipids, leading to disorders associated with neurological problems, such as Alzheimer's disease and Wilson's disease, while a deficiency of Cu^{2+} is associated with the complications of genetic defects, colon cancer, and cardiovascular disease.[7–10] On the other hand, cysteine (Cys), an essential thiol-containing amino acid, plays vital roles in protein synthesis, detoxification, post-translational control, and metabolism.[11,12] In addition, as a potential biomarker for various diseases, abnormal intracellular levels of Cys have been correlated with Parkinson's disease, cardiovascular disease, Alzheimer's disease, liver damage, as well as developmental retardation.[13,14] It is worth pointing out that Cys is a strong Cu^{2+} binder and can remove Cu^{2+} from sensors.[15] In this regard, developing effective strategies aiming at simultaneously monitoring cellular Cu^{2+} and Cys are highly meaningful for human-health.

Luminescence approach based on the use of suitable probes has become an excellent choice for detecting cations, anions, and other bioactive species, owing to its high sensitivity, selectivity, real-time detection, high spatiotemporal resolution, operational simplicity, and non-invasiveness in biological samples.[16–18] Many luminescence probes have been successfully developed to detect Cu^{2+} and Cys, most of them are reaction based chemical sensors on the basis of various mechanisms.[19,20] Unfortunately, most of the organic reactions are time-consuming, poorly selective, and require relatively strict conditions, which limit the usefulness of the probes. As another promising designing strategy, a Cu^{2+}-displacement approach is adopted by the Cys probe[21,22] based on the formation of a Cys–Cu^{2+} complex through a Cu–S bond, which has a larger stability constant than that of the $[Cu\text{-probe}]^{2+}$ complex. This Cu^{2+}-

[a]School of Chemistry and Chemical Engineering, Guangdong Pharmaceutical University, Zhongshan, 528458, P. R. China. E-mail: xuli473@163.com; Fax: +86-760-88207266; Tel: +86-760-88207266

[b]School of Food and Biological Engineering, Hefei University of Technology, Hefei, 230009, P. R. China. E-mail: fengw420@hfut.edu.cn

† Electronic supplementary information (ESI) available. See DOI: 10.1039/d0ra10794h

‡ These authors contributed equally to this work.

displacement strategy offers an alternative way of achieving a quick and direct method for assaying Cys through "off–on" fluorescent signaling resulting from Cu^{2+} displacement. Some Cu^{2+}-based ensemble probes for detecting Cys have been reported, including those that rely on phenanthraquinone, coumarin, naphthalimide, naphthol, zwitterionic polythiophene derivatives. However, these fluorescent probes are mainly organic dyes that have some notable optical shortcomings.[23–25] Moreover, reports on probes capable of tracking Cys at subcellular levels are scarce, especially for visualizing Cys levels in mitochondria.

Transition metal complexes, as luminescence probes for various analytes, have been extensively investigated in living systems.[26,27] In particular, cyclometalated iridium(III) complexes exhibit high photoluminescence efficiencies, relatively long emission lifetime, distinct emission color tunability through ligand-structure control, and high photostability for bioimaging experiments.[28] They have emerged as novel and promising luminescent probes for biomolecules and metal ions.[29] Recently, some cyclometalated iridium(III) complexes have been investigated for their abilities to detect Cu^{2+} or biological thiols.[30–33] However, to the best of our knowledge, none of these complexes have been applied to the simultaneous detection of cellular Cu^{2+} and Cys. Herein, a novel luminescent iridium(III) complex (Ir) for the sequential detection of Cu^{2+} and Cys was designed. The incorporation of pyrazolyl-pyridine ligand was designed as Cu^{2+} recognition unit, following by the Cu^{2+}-displacement strategy to detect Cys. The proposed displacement mechanism was elucidated by ^{1}H NMR spectroscopy and electrospray ionization mass spectroscopy (ESI-MS). Ir selectively accumulated in mitochondria and was used to detect and image Cu^{2+} and Cys, both *in vitro* and *in vivo*, using a sequential method. In addition, Cu^{2+} and Cys were quantitatively luminescence-monitored at the subcellular level by flow cytometry. The *in vitro* and *in vivo* confocal microscopy and flow cytometry results for Ir showed that endogenous Cys could be detected. This newly developed luminescence probe is a potentially useful tool for imaging and detecting Cu^{2+} and Cys in a wide range of physiological and pathological processes.

2 Experimental section

2.1 Materials and instruments

2-Phenylpyridine (ppy), 1,4-bis(bromomethyl)naphthalene, 3(2-pyridyl)pyrazole, *N*-2-hydroxyethylpiperazine-*N*′-2-ethanesulfonic acid (HEPES), $IrCl_3$ and all the other metal salts and amino acids were obtained from Sigma-Aldrich and used without further purification. The cell culture media, reagents, and 3-(4,5-dimethylthiazol-2-yl)-2,5-diphenyltetrazoliu bromide (MTT) were purchased from Sangon Biotech (Shanghai, China). Mito Tracker® Red FM (MTR) was purchased from Invitrogen. The ligand L^{14naph} (ref. [34]) and the compound $[Ir(ppy)_2Cl]_2$ (ref. [35]) were synthesized and purified as the previously reported literatures.

^{1}H and ^{13}C NMR spectra were acquired on a Bruker 400 MHz NMR spectrometer using tetramethylsilane (TMS) as internal standard. Electrospray ionization MS (ESI-MS) were performed on a LCQ system (Finnigan MAT, USA). Elemental analyses were carried out on a Perkin-Elmer 240Q elemental analyzer. Absorption spectra were measured on a Varian Cary 300 spectrophotometer. Steady-state emission measurements were taken on an Edinburgh instrument FLSP-920 spectrometer with a Xe lamp as an excitation source. Phosphorescence lifetimes were performed on an Edinburgh FLSP-920 photo-counting system using a hydrogen-filled lamp as the excitation source. Phosphorescence quantum yield of Ir was measured in a PBS buffer solution (pH = 7.4) and calculated by comparison with the reference $[Ru(bpy)_3]^{2+}$.[36]

2.2 Synthesis of $[Ir(ppy)_2L^{14naph}]Cl$ (Ir)

$[Ir(ppy)_2Cl]_2$ (107.2 mg, 0.1 mmol) and ligand L^{14naph} (88.4 mg, 0.2 mmol) were heated in a mixed solution of $CH_3OH/CHCl_3$ (1 : 1, v/v; 20 mL) at 65 °C for 6 h under an argon atmosphere. The solvent was removed by rotary evaporation, and the crude product was purified by column chromatography on a neutral alumina using CH_2Cl_2 and MeOH (8 : 1, v/v) as eluent, to get Ir. Yield: 147.7 mg, 75.5%. Anal. calc. for $C_{50}H_{38}N_8ClIr$ (%): C, 61.37; H, 3.91; N, 11.45; found(%): C, 61.85; H, 3.87; N, 11.03. ES-MS [CH_3OH, *m*/*z*]: 943.7($[M - Cl^-]^+$). ^{1}H NMR (400 MHz, DMSO) δ 8.50 (d, J = 4.6 Hz, 1H), 8.38 (d, J = 8.0 Hz, 1H), 8.20 (d, J = 8.5 Hz, 1H), 8.14–8.02 (m, 3H), 7.98–7.85 (m, 3H), 7.85–7.76 (m, 2H), 7.72 (d, J = 7.8 Hz, 1H), 7.65 (t, J = 7.7 Hz, 1H), 7.61–7.49 (m, 3H), 7.46 (d, J = 5.5 Hz, 1H), 7.41–7.33 (m, 1H), 7.32–7.20 (m, 3H), 7.16 (d, J = 8.1 Hz, 1H), 7.02 (dd, J = 12.8, 7.1 Hz, 2H), 6.92 (q, J = 6.2 Hz, 2H), 6.74 (t, J = 7.4 Hz, 1H), 6.41 (dd, J = 15.9, 7.9 Hz, 2H), 6.28 (d, J = 7.4 Hz, 1H), 6.03 (t, J = 7.9 Hz, 2H), 5.85–5.68 (m, 4H), 5.39 (dd, J = 34.5, 12.1 Hz, 2H). ^{13}C NMR (101 MHz, DMSO) δ 167.47, 167.11, 153.35, 152.24, 152.10, 151.70, 150.03, 148.39, 146.63, 144.60, 144.21, 138.32, 138.08, 133.75, 133.51, 133.27, 130.98, 129.90, 127.58, 127.40, 125.76, 123.91, 122.24, 120.75, 120.36, 108.00, 105.28, 53.49.

2.3 Synthesis of $[Ir(ppy)_2L^{14naph}CuCl_2]Cl$ (Ir–Cu)

$[Ir(ppy)_2L^{14naph}]Cl$ (244.6 mg, 0.25 mmol) and $CuCl_2$ (33.2 mg, 0.25 mmol) were suspended in methanol (20 mL) and stirred for 2 h at room temperature. The Ir–Cu complex was precipitated by adding ether into the solution, isolated by filtration, and dried under vacuum (166.7 mg, 60%). ES-MS: *m*/*z* (CH_3OH): 1076.3 [M + 2Cl + Cu − H]$^+$; anal. calc. for $C_{50}H_{38}Cl_3N_8CuIr$ (1111.1) (%): C 53.96, H 3.44, N 10.07; found: C 53.87, H 3.56, N 10.15.

2.4 General procedure for the spectrum measurement

A stock solution of Ir (1 mM) was prepared in DMSO. The metal ion stock solutions (10 mM) were prepared using their nitrate salts or chloride salts (Na^+, Ag^+, K^+, Mg^{2+}, Zn^{2+}, Ni^{2+}, Co^{2+}, Cd^{2+}, Hg^{2+}, Cu^{2+}, Ca^{2+}, Pb^{2+}, Fe^{3+}, Al^{3+} and Cr^{3+}) in twice-distilled water. Stock solutions (10 mM) of (Cys, Gly, Hcy, GSH, Cys–Cys, Ala, Glu, Arg, Lys, Tyr, His, Phe, Leu, Val, Ser, Met, and Pro) by direct dissolution in double distilled water were prepared. These stock solutions were further diluted to required concentration for measurement.

Absorption and emission spectra were obtained using Ir (5 μM) in HEPES solution (pH 7.4) with the analytes at various

concentrations at room temperature. The phosphorescence spectra were recorded under 376 nm excitation wavelength.

The total concentration of Cu^{2+} ions and Ir remained constant (10 μM). Then the phosphorescence intensity of Ir was recorded by changing the molar ratio of the Ir to Cu^{2+}.

The selectivity studies of Ir for Cu^{2+} were tested by comparing other metal ions. Ir (5 μM) was treated with Cu^{2+} ions (5 μM) and other metal ions (30 μM) for 10 min and the phosphorescence intensity of the mixtures was recorded.

The phosphorescence spectra for the evaluation of the selectivity of Ir–Cu ensemble (5 μM) for Cys (10 μM) was measured by adding various interfering amino acids (30 μM) into the solutions of Cys and the remaining detection conditions were the same as described above.

For reproducibility tests, Cu^{2+} ions (5 μM) were incubated with Ir aqueous solution (5 μM), and the phosphorescence of Ir was quenched. Then, by the addition of Cys (10 μM), the phosphorescence of Ir was recovered. Ir was resuspended after removing Cys and Cu^{2+} ions by centrifugation and the same experimental procedure was repeated five times.

The phosphorescence intensity of Ir (5 μM), Ir–Cu ensemble (5 μM) and Ir–Cu ensemble (5 μM) with Cys (10 μM) was determined in a series of buffers with pH ranging from 1 to 12.

2.5 Cell and zebrafish culture

HeLa cells were obtained from the Cell Bank (Cell Institute, Sinica Academica Shanghai, Shanghai, China) and were incubated using Dulbecco's modified Eagle's medium (DMEM) with addition of 10%(v/v) fetal bovine serum (FBS) and 1% penicillin/streptomycin in a humidified atmosphere of 5% CO_2 at 37 °C incubator. Sexually mature zebrafish were selected for spawning. They were bred and maintained for up to 5 days. More details on the HeLa cells and zebrafish experiments are given in the ESI.†

3 Results and discussion

3.1 Synthesis and characterization

Ir was synthesized through $[Ir(ppy)_2Cl]_2$ and the corresponding L^{14naph} ligand in a stoichiometric amount. Ir purification was performed by aluminium oxide chromatography with $CHCl_3$ and CH_2OH as the eluents, and the complex was characterized by ESI-MS, ^1H and ^{13}C NMR spectroscopy (Fig. S1–S3†). The data obtained are in good agreement with the proposed structures. In addition, the synthetic process is simple and facile without requiring tedious purification.

3.2 Phosphorescence response of Ir to Cu^{2+}

The designed mononuclear Ir bears an extra chelation ligand, which has the potential ability for recognizing metal ions. We investigated the phosphorescent response of Ir in HEPES solution against various metal ions. As shown in Fig. 1A, upon addition of Cu^{2+}, the color of Ir solution changed from strong green to black when exposed to UV light (365 nm). However, the addition of other metal ions (such as Hg^{2+}, Ni^{2+}, Ag^{+}, Co^{2+}, K^{+}, Na^{+}, Al^{3+}, Ca^{2+}, Fe^{3+}, Zn^{2+}, Cd^{2+}, Cr^{3+}, Mg^{2+} and Pb^{2+}) showed negligible effect on the phosphorescence intensity of Ir. These initial results indicated that Ir can specifically detect Cu^{2+} over other tested metal ions. The phosphorescence titration experiments were subsequently carried out to examine the sensitivity of Ir towards Cu^{2+} ions. As shown in Fig. 1B, the phosphorescence intensity of Ir (5 μM) at 486 nm gradually decreased as the Cu^{2+} concentration was increased from 0 to 2 equiv. The maximum phosphorescence quenching efficiency of Ir was determined to be ~90% after the addition of 1 equiv. of Cu^{2+}. The phosphorescence intensity of Ir at 486 nm varied linearity with Cu^{2+} concentrations (R^2 = 0.995; 20 nM to 1.5 μM) (Fig. 1C), and the limit of detection (LOD) of Ir for Cu^{2+} was calculated to be ~20 nM using the equation of $3\sigma/k$, which was much lower than the safety limit of copper ions in drinking water set by EPA (20 μM) and WHO (30 μM),[37] which indicated that Ir had high sensitivity to Cu^{2+}.

To investigate the selectivity of Ir, the phosphorescence responding at 5 μM toward various metal ions were examined using emission spectroscopy under the same conditions. As shown in Fig. 1D, significant phosphorescence quenching was observed when Cu^{2+} was added, while no obvious phosphorescence changes observed with other metal ions. The good selectivity of Ir can be attributed to the suitable geometry, proper ionic radius, and sufficient binding energy of the copper ion.[38] However, other metal ions could not satisfy these characteristics. They could not combine with Ir and annihilate phosphorescence. Furthermore, we also evaluated the anti-interference ability of Ir (5 μM) to Cu^{2+} (10 μM) in the presence of other metal ions (30 μM) (Fig. S4†). The results showed that there were no obvious changes in the phosphorescence intensity. The phosphorescence responses of Ir to mixtures of Cu^{2+} and other background metal ions were almost identical to pure Cu^{2+}. Through the above experiment, the sensing of Cu^{2+} was hardly interfered by these coexisting metal ions and Ir had high selectivity and excellent anti-interference ability for detection of Cu^{2+}.

In addition, a Job's plot from phosphorescence titration spectra revealed a 1 : 1 stoichiometric relationship between Ir and Cu^{2+} (Fig. 1E). The response times of Ir (5 μM) toward various concentrations of Cu^{2+} (0.5–2.5 μM) was examined in HEPES buffer (pH 7.4). As shown in Fig. S5,† all concentrations of Cu^{2+} exhibited maximum phosphorescence intensities within 30 s. This kinetic analysis revealed that Ir responded in a manner that was almost independent of Cu^{2+} concentration. Hence, Ir is potentially a powerful tool for the rapid detection of Cu^{2+}.

3.3 Phosphorescence response of the Ir–Cu ensemble towards Cys

Since Cu^{2+} can strongly bind to Cys, the ability of Ir–Cu ensemble to detect Cys was explored. Hence, we prepared the ensemble by adding an equal amount of Cu^{2+} to Ir solution and investigated its phosphorescence towards Cys. As shown in Fig. 2A, the phosphorescence color of the ensemble changed from black to bright green exclusively in the presence of Cys, while other amino acids did not result in any color change, when the ensemble irradiated with UV light at 365 nm. Fig. 2B

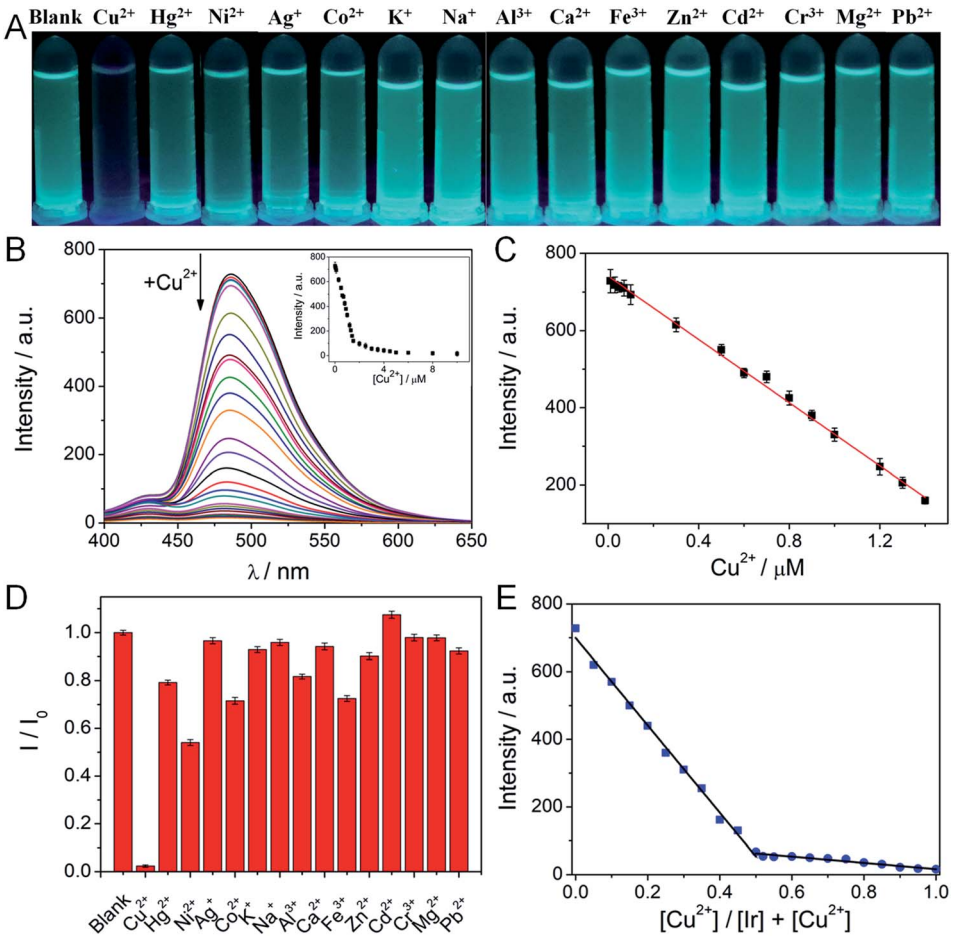

Fig. 1 (A) The photograph of Ir (5 μM) in the presence of various metal ions (10 μM) under 365 nm UV lamp. (B) Phosphorescence spectra of Ir (5 μM) with the addition of Cu^{2+} (0–10 μM) in HEPES buffer (pH 7.4). Inset: the phosphorescence intensity at 486 nm decreased upon adding Cu^{2+}. (C) Initial linear phosphorescence responses at low Cu^{2+} concentrations. (D) Phosphorescence responses of Ir (5 μM) to different metal ions (10 μM each). (E) Job's plot of Ir with Cu^{2+} according to the method of continuous variations. The sum of the total molar concentration of Cu^{2+} and Ir was constant.

showed that phosphorescence at 486 nm strongly enhanced as Cys (0–2 equiv.) was gradually added which had a 31-fold increase in phosphorescence intensity. This observation was due to the release of Ir. The Ir–Cu ensemble responded linearly to Cys ($R^2 = 0.994$), with a low detection limit of 54 nM (Fig. 2C), which was comparable or even superior to those of recently reported fluorescence probes for Cys detection (Table S1†).

To investigate the selectivity of the Ir–Cu ensemble towards Cys, the emission spectra of Ir–Cu ensemble with 17 different amino acids were measured. As shown in Fig. 2D and E, apart from the Cys, various amino acids including Gly, Hcy, GSH, Cys–Cys, Ala, Glu, Arg, Lys, Tyr, His, Phe, Leu, Val, Ser, Met, and Pro had no obvious influence on the phosphorescence spectra of Ir–Cu ensemble. This result was of significance since the Cys detection was generally interfered by Hcy and GSH. The specifical selectivity to Cys of Ir–Cu ensemble might be due to two possible factors. First, the pK_a value of the thiol group in the side chain in Cys (8.00) was lower than those in Hcy (8.87) and GSH (9.20).[39] At pH 7.4, Cys existed predominantly in the form of thiolate and had a superior affinity for Cu^{2+} than other two biothiols. The steric hindrance of the thiol group of Cys was smaller than that of Hcy and GSH, which could be another possible factor for the selectivity to Cys of Ir–Cu ensemble.[40] In addition, as shown in Fig. S6,† the competition experiments revealed that the presence of other amino acids did not interfere with the ability of the Ir–Cu ensemble to detect Cys.

The phosphorescence intensity of the ensemble was observed to change with time, as shown in Fig. S7,† the maximum phosphorescence response was almost immediately observed upon interacting with 0.1–2 equiv. of Cys. The recovered phosphorescence intensity remained constant as the incubation time was extended from 1 to 10 min.

3.4 Effect of pH, time-dependent and recyclability studies

To determine the potential biological applications of the developed system, the influence of pH on the phosphorescence response of Ir toward Cu^{2+} and Cys was investigated. As shown in Fig. S8,† the phosphorescence intensity of Ir (5 μM) did not change in the pH ranging from pH 6 to pH 12, which indicated that Ir was very stable in a relatively wide pH range. A remarkably lower phosphorescence intensity was observed in the

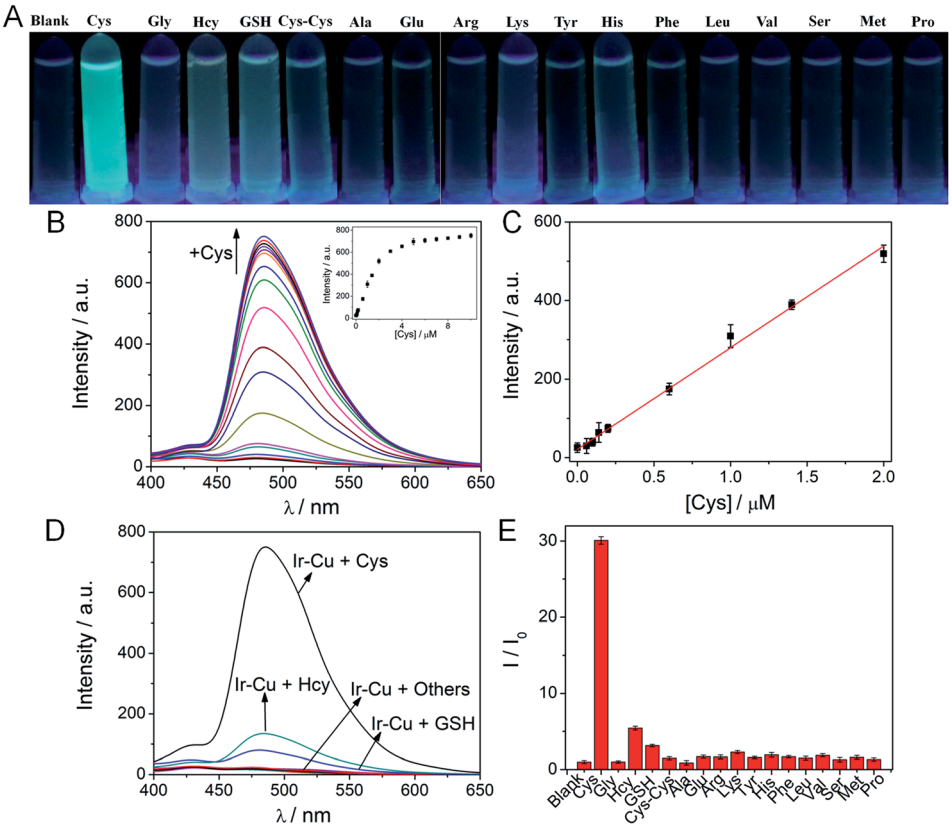

Fig. 2 (A) Photograph of Ir–Cu ensemble (5 μM) in the presence of various amino acids (10 μM) under 365 nm UV lamp. (B) Phosphorescence spectra of Ir–Cu ensemble (5 μM) upon addition of Cys (0–10 μM) in HEPES buffer (pH 7.4). Inset: the phosphorescence intensity changes of Ir–Cu ensemble (5 μM) upon addition of Cys. (C) Initial linear phosphorescence responses at low Cys concentrations. (D) Phosphorescence spectra of Ir–Cu ensemble (5 μM) to various amino acids (10 μM) in HEPES buffer (pH 7.4). (E) Phosphorescence responses of Ir–Cu ensemble to different amino acids (10 μM each).

presence of Cu^{2+} over a wide pH range (pH 1–12), which demonstrated that the complex effectively coordinated to Cu^{2+} under both acidic and alkaline conditions. Furthermore, the phosphorescence response of the Ir–Cu ensemble to Cys was also shown to be pH-dependent, with emission recovery observed in the pH ranging from pH 5 to pH 11. Therefore, Ir was suitable for sequentially detecting Cu^{2+} and Cys in the biologically relevant pH range.

The time course of the response of Ir to Cu^{2+}/Cys sequential detection was carried out. As shown in Fig. S9,† the phosphorescence intensity of Ir was essentially stable in HEPES solution (pH 7.4), which indicated that Ir was very soluble and stable under aqueous conditions. However, the emission of Ir was rapidly quenched within 30 s upon addition of Cu^{2+} and then remained almost unchanged thereafter. The subsequent phosphorescence recovery process, owing to the Cys binding and Ir release, was also accomplished immediately (<30 s) under the same conditions. These results demonstrated that Ir and the Ir–Cu ensemble are suitable for the real-time detection of Cu^{2+} and Cys, respectively.

Reversibility is a vital feature of a probe used to detect analytes in practical applications. A switchable change in the phosphorescence intensity of Ir at 486 nm could be repeated, without signal loss, by alternately adding Cu^{2+} and Cys in HEPES solution (Fig. S10†), which indicated that Ir can be developed as a reversible "on–off–on" phosphorescence probe for Cu^{2+} and Cys.

3.5 Proposed mechanism

Ir complex exhibited an interesting "on–off–on" three state emission with the stepwise addition of Cu^{2+} and Cys. As shown in Scheme 1, the addition of Cu^{2+} can result in phosphorescence quenching accompanied by a bright-green to dark color change, which was attributed to its chelation with the pyrazolyl-pyridine groups of Ir and the formation of the Ir–Cu ensemble. The phosphorescence quenching property stems from the paramagnetic nature of Cu and the coordination of Cu^{2+} provides a pathway for nonradiative deactivation of the excited state of Ir.[36] Due to the stronger binding interaction of Cu^{2+} with Cys, Cys captured Cu^{2+} from Ir, resulting in phosphorescence revival and a dark to green color change. During this process, the phosphorescence of Ir changes from "on" to "off" and then "on" again.

The sensing mechanism was examined by ^1H NMR spectroscopy, ESI-MS, phosphorescence-lifetime and UV-visible absorption spectroscopy. The ^1H NMR spectrum of the solution exhibited very broad peaks when Cu^{2+} was added to Ir in DMSO-d_6–D_2O (4 : 1 v/v), which eventually vanished due to the

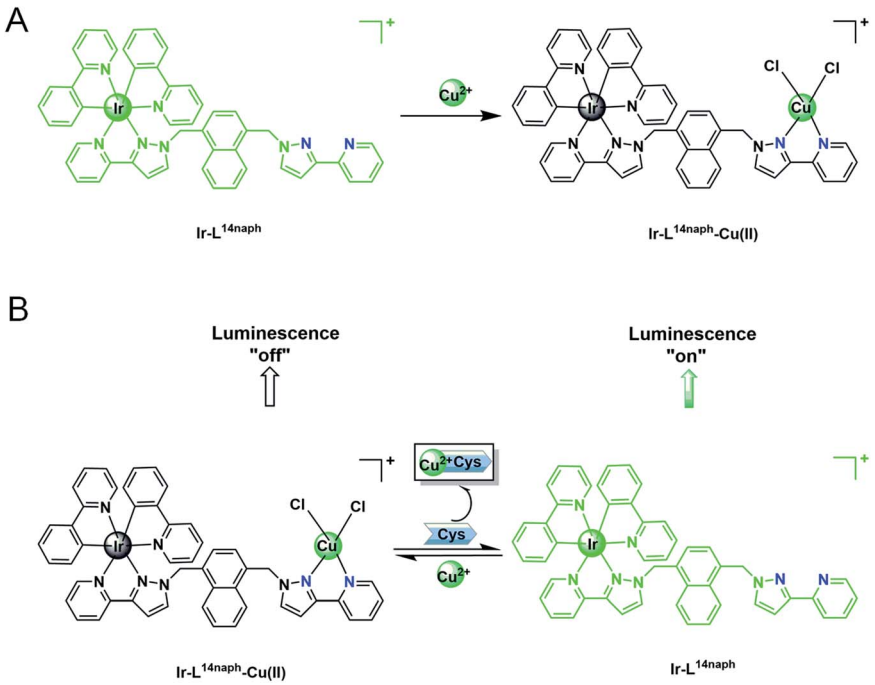

Scheme 1 (A) Chemical structures of Ir and Ir–Cu ensemble; counterion Cl^- was omitted for clearity. (b) Illustration of the design of a reversible Ir-based phosphorescence probe Ir–Cu ensemble for Cys detection.

coordination of paramagnetic Cu^{2+} with Ir.[41] However, the ^1H NMR spectrum recovered when the Ir–Cu ensemble was treated with Cys, which indicated that Cys was able to extract Cu^{2+} from the ensemble (Fig. 3). To further investigate this mechanism, the Ir–Cu ensemble and the Ir–Cu ensemble in the presence of Cys were measured by ESI-MS. As shown in Fig. S11,† signals corresponding to $[Ir + Cu + H^+]^{2+}$, $[Ir + Cu + 2Na^+ - H^+]^{2+}$, $[Ir + Cu + Na^+ + Cl + H_2O]^{2+}$, and $[Ir + Cu + 2Cl]^+$ were observed in the spectrum when 1 equiv. of Cu^{2+} was added to Ir, with the peak corresponding to Ir notable absent. These results also suggested that Ir was coordinated to Cu^{2+} in a 1 : 1 binding mode. In addition, a peak was observed at 943.68 in the spectrum of the Ir–Cu ensemble/Cys, which corresponds to that of Ir. These results were consistent with the proposed mechanism shown in Scheme 1. The phosphorescence quenching mechanism is divided into dynamic quenching (collision induced quenching) and static quenching (forming ground-state complex between the quencher and fluorophore). The phosphorescence quenching types can be effectively confirmed by phosphorescence lifetime.[42] We conducted a phosphorescence-decay experiment, with the lifetimes of Ir, Ir–Cu ensemble and Ir–Cu ensemble/Cys determined to be 1184.9, 1146.8, and 1156.7 ns, respectively, by fitting the data to single exponential decay functions (Fig. S12†). Using $[Ru(bpy)_3]^{2+}$ as a reference, the phosphorescence quantum yields of the Ir, the Ir–Cu ensemble, and the Ir–Cu ensemble/Cys were determined to be 0.126, 0.118 and 0.122, respectively. Since the phosphorescence lifetime of Ir was the same before and after titrating with Cu^{2+}, we speculated that Cu^{2+} coordinated with the bidentate chelating pyrazolyl-pyridine group of Ir to form a non-luminescent Ir–Cu ensemble that caused static quenching.[43] Furthermore, in order to further assist in demonstrating the static quenching mechanism proposed above, UV-vis absorption spectra of Ir were explored before and after adding Cu^{2+} (Fig. S13†). The absorbance of the band at 250 nm increased, but the band at 340 nm and 376 nm decreased, and a prominent isosbestic point at 308 nm appeared, suggesting the formation of a complex system between Ir and Cu^{2+}. After the addition of Cys, the absorption peak position of the solution corresponded to the absorption peak of only Ir alone. This result may be because Cys destroyed the coordination bond formed by Cu^{2+} and Ir. This provides further strong evidence for the static quenching mechanism.

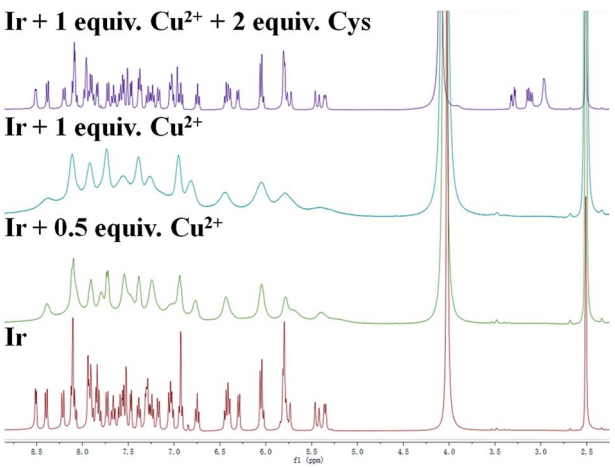

Fig. 3 ^1H NMR 400 MHz spectra of Ir (5 mg) in the presence of 0, 0.5, or 1 equiv. Cu^{2+} and sequential 2 equiv. Cys in DMSO-d_6–D_2O (4 : 1 v/v).

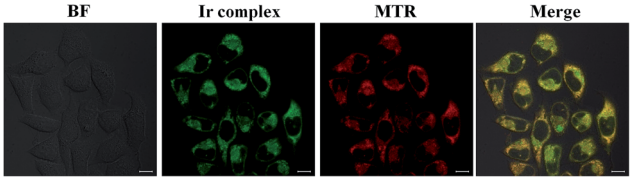

Fig. 4 Confocal images of HeLa cells treated with Ir (5 μM) for 1 h at 37 °C, then incubated with MTR (50 nM, 0.5 h). Scale bar: 10 μm.

3.6 Phosphorescence detection of Cu^{2+} and Cys in live cells

Cytotoxicity, bioimaging, and flow cytometry experiments were carried out to further evaluate the ability of Ir to practically monitor Cu^{2+} and Cys in biological systems. We first assessed the cytotoxicity of Ir to HeLa cells using an MTT assay and the data are shown in Fig. S14.† Above 90% of the cells were viable after being treated with Ir (0–30 μM) for 24 h, demonstrating that Ir was very biocompatible.

We next investigated the cellular distribution of Ir by co-localization and ICP-MS experiments. As shown in Fig. 4, the phosphorescence images of Mito-Tracker Red (MTR) and Ir exhibited good overlap, with a Pearson's correlation coefficient of 0.92, which suggests that Ir was mainly localized in the mitochondria of HeLa. The amounts of iridium present in the cellular organelles (*i.e.*, nucleus, mitochondria, and cytoplasm) were further determined by ICP-MS experiments. Fig. S15† revealed substantial differences between each organelle, with more than 91% of the iridium localized in the mitochondria, which indicated that Ir significantly targeted the mitochondria. The photostabilities of Ir and commercially available MTR were confirmed by the photobleaching experiment in living HeLa cells. Fig. S16† showed that, when irradiated, the phosphorescence intensity of Ir decreased by ~20% after 160 s, while MTR phosphorescence decreased by 90% after 160 s. Therefore Ir performed outstandingly photostable compared to MTR for bioimaging purposes. Taken together, the high *in vitro* selectivity for Cu^{2+} and Cys and good biocompatibility of Ir encouraged us to further investigate the phosphorescence detection of Cu^{2+} and Cys in mitochondria using Ir as a chemosensor.

We next turned to evaluate the ability of Ir to detect Cu^{2+} and Cys in live cells by confocal microscopy and flow cytometry. To demonstrate that the phosphorescence of Ir responded reversibly to Cu^{2+} and Cys, HeLa cells were incubated with Ir (5 μM, 1 h) at 37 °C, and Ir-loaded cells were then sequentially treated with Cu^{2+} and Cys. Fig. 5 showed the phosphorescence imaging and flow cytometry results for Cu^{2+} and Cys in live HeLa cells. The HeLa cells initially exhibited strong green phosphorescence after being incubated with Ir for 1 h. Ir-loaded HeLa cells were

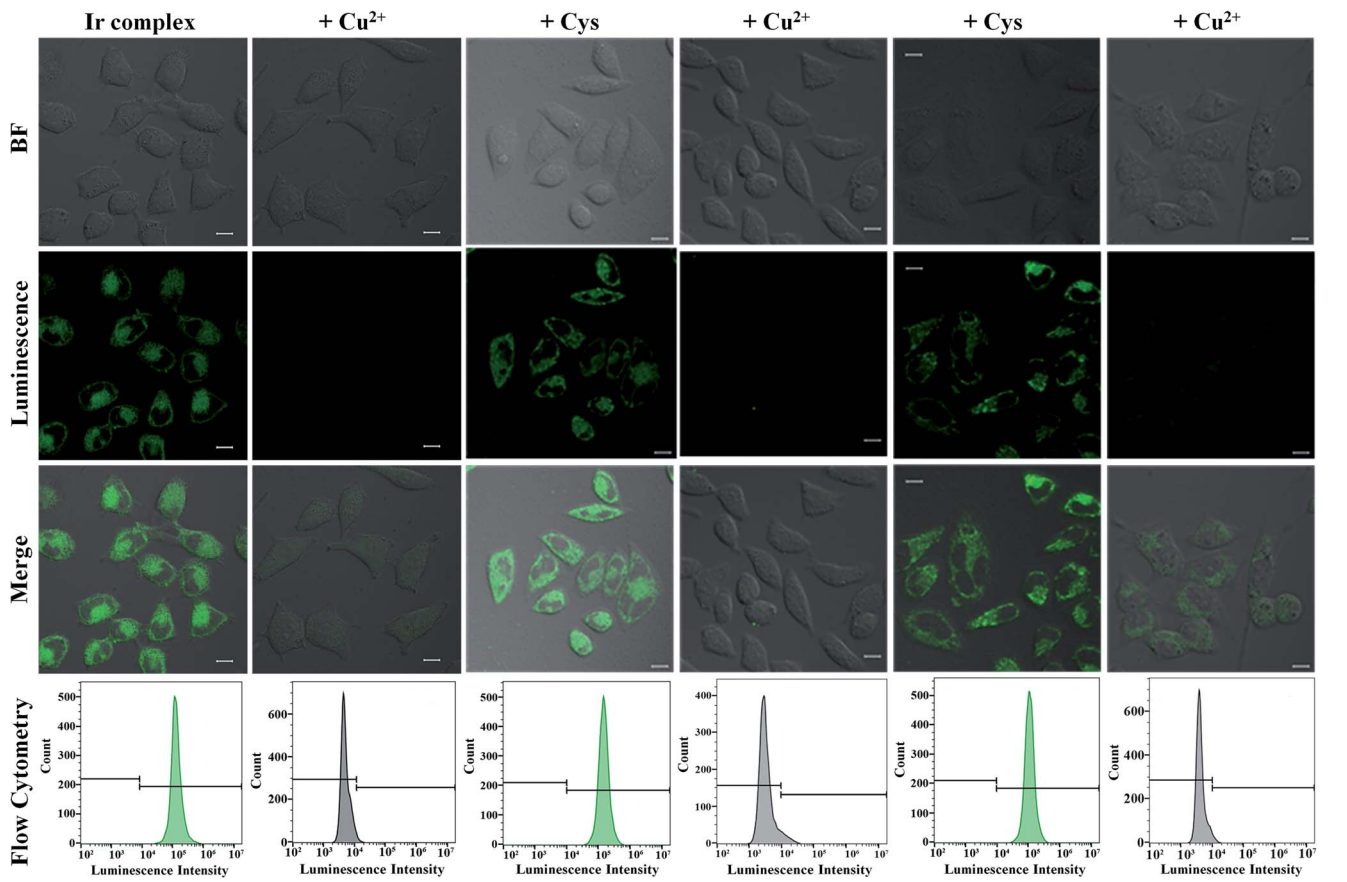

Fig. 5 Confocal microscopic and flow cytometric analysis of "on–off–on" cycles in HeLa cells. Cells were pre-stained with Ir (5 μM, 1 h) and Cu^{2+} ions (5 μM, 0.5 h), and then incubated with Cys (10 μM, 0.5 h). The mean phosphorescence intensity in cells was determined using flow cytometric analysis with excitation at 405 nm. Scale bar: 10 μm.

then treated with Cu^{2+} for 0.5 h, which resulted in the complete quenching of their green phosphorescence, showing that Ir responded rapidly to Cu^{2+} and that the non-phosphorescent Ir–Cu ensemble was formed in the live cells. Intense green phosphorescence was recovered when these cells were pre-stimulated with exogenous Cys for 0.5 h, which demonstrated that the Ir–Cu ensemble interacted with Cys. To further quantitatively study the reversible phosphorescence in response to Cu^{2+} and Cys in live cells, the flow cytometry experiments was carried out to measure the phosphorescence of 10 000 cells from each population. Fig. 5 displayed the phosphorescence signals of live HeLa cells stained with Ir and then incubated with Cu^{2+} and Cys. As a control group, HeLa cells showed negligible background phosphorescence signals. The mean phosphorescence intensity of HeLa cells gradually declined with increasing Cu^{2+} concentration (Fig. S17†), but then increased with increasing Cys concentration (Fig. S18†).

Next we turned our attention to detecting endogenous Cys in live HeLa cells with the Ir–Cu ensemble. As shown in Fig. 6, a certain amount of cellular green phosphorescence was produced in HeLa cells after incubation with the Ir–Cu ensemble for 1 h, which was ascribed to the reaction between the ensemble and endogenous Cys. Moreover, markedly lower phosphorescence was observed by confocal microscopy when HeLa cells were stimulated by 0.5 mM *N*-ethylmaleimide (NEM), a thiol blocking reagent for 1 h and then treated with the Ir–Cu ensemble (5 μM) for 1 h. Finally, we further examined the selectivity of the Ir–Cu ensemble toward Cys over other thiols by successively incubating NEM, Cys, Hcy or GSH, and the Ir–Cu ensemble, with intracellular Cys showing stronger green phosphorescence. Meanwhile, the confocal microscopy results were further supported by quantitative flow cytometry data (Fig. S19†). In addition, different concentrations of NEM were added into the cells to reduce the concentration of intracellular Cys before incubation with the Ir–Cu ensemble. The mean phosphorescence intensity gradually decreased with increasing of NEM concentrations (Fig. S20†). These results demonstrated that the Ir–Cu ensemble responded to endogenous Cys in live cells.

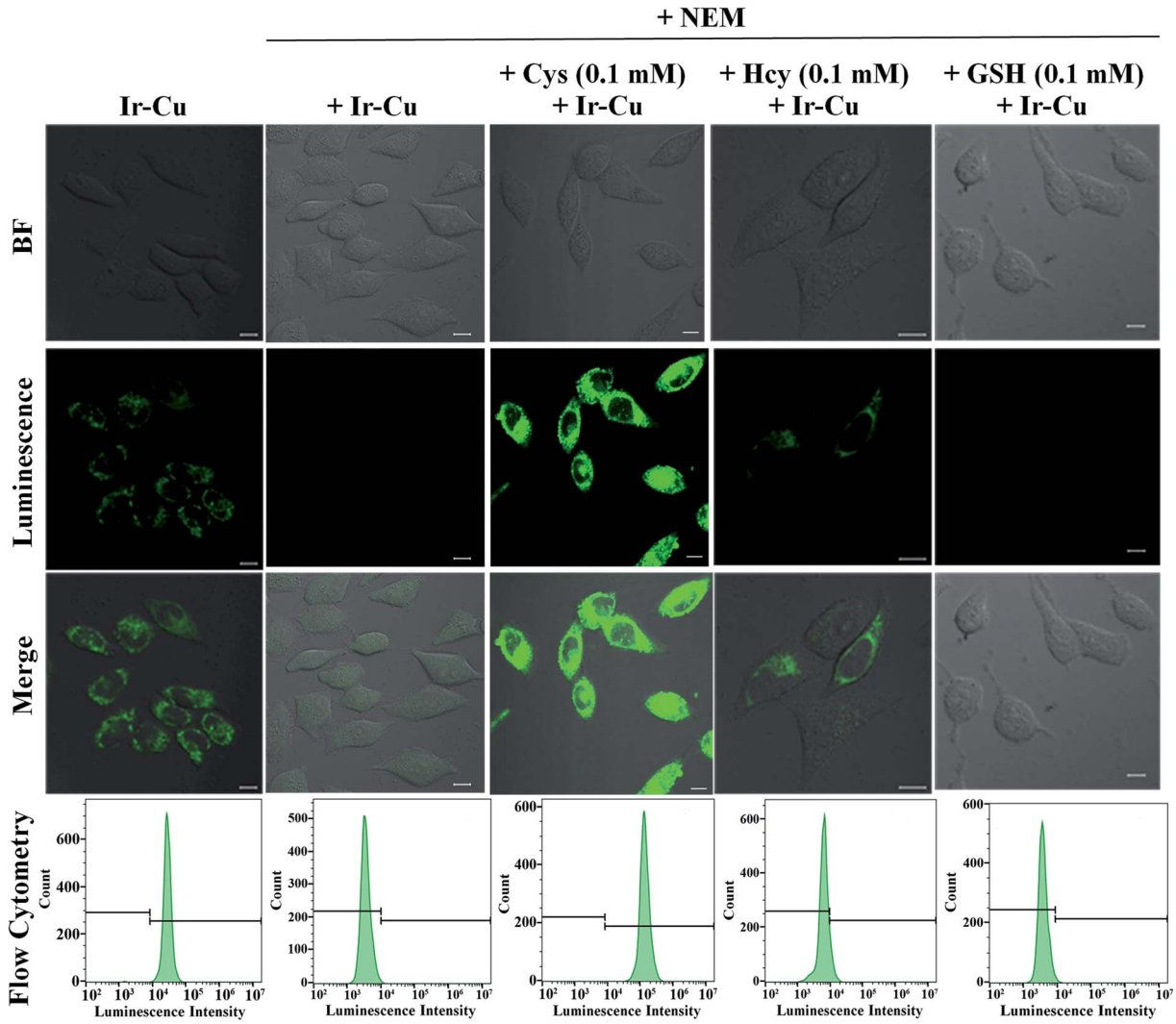

Fig. 6 Confocal microscopic and flow cytometric analysis of HeLa cells. HeLa cells stained with Ir–Cu ensemble (5 μM, 1 h) or HeLa cells pretreated by the NEM (0.5 mM, 0.5 h), and then stained by Cys, Hcy, and GSH (0.1 mM, 0.5 h), followed up by treating with Ir–Cu ensemble (5 μM) for 1 h. Scale bar: 10 μm.

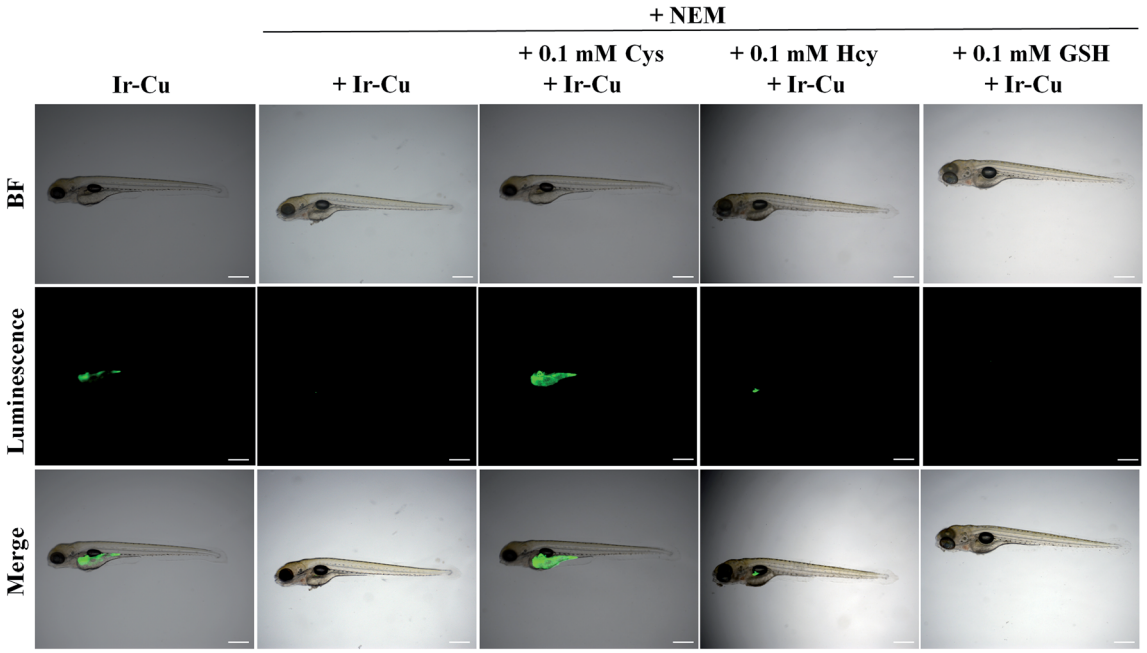

Fig. 7 Phosphorescence images of zebrafish. Zebrafish treated with Ir–Cu ensemble (5 μM) for 1 h, zebrafish pre-incubated with NEM (0.5 mM) for 0.5 h, and then treated with Cys (0.1 mM), Hcy (0.1 mM) and GSH (0.1 mM) for 0.5 h, respectively, followed by Ir–Cu ensemble (5 μM) for 1 h. Scale bar = 500 μm.

3.7 Imaging of Cys in living zebrafish

Zebrafish were chosen as the animal model to assess the feasibility of Ir–Cu ensemble to detect Cys *in vivo* (Fig. 7). Five-day-old zebrafish exhibited significant green phosphorescence by incubating with the Ir–Cu ensemble (5 μM) for 1 h. In contrast, no phosphorescence was observed after the zebrafish were pre-incubated with NEM (0.5 mM) for 0.5 h and then with the Ir–Cu ensemble (5 μM) for another 1 h. In addition, the phosphorescence signal was restored by Cys, while Hcy and GSH did not produce any significant change when the zebrafish was treated with NEM, biothiols, and the Ir–Cu ensemble in a step-by-step manner for 0.5 h, 0.5 h, and 1 h, respectively. These results demonstrated that the Ir–Cu ensemble can be used to image endogenous Cys in zebrafish.

4 Conclusions

We synthesized a new Ir(III) complex as a phosphorescent probe that uses the displacement approach to sequentially recognize Cu^{2+} and Cys. Ir responded rapidly, was highly selective, showed excellent sensitivity for the detection of Cu^{2+}, and served as an "on–off"-type probe. The *in situ*-generated Ir–Cu ensemble was sequentially well used as an "off–on" phosphorescence probe for the specific detection of Cys, with the sensing mechanism further demonstrated to involve a static quenching process. Ir exhibited low cytotoxicity and mitochondria-targeting properties, and was able to reversibly phosphorescence-image Cu^{2+} and Cys in the mitochondria of living cells. In addition, subcellular Cu^{2+} and Cys were quantitatively phosphorescence detected by flow cytometry. Finally, the Ir–Cu ensemble was successfully used to image endogenous and exogenous Cys in a zebrafish model. As we know, this is the first example that the newly developed Ir–Cu ensemble is used for investigating endogenous Cys in *in vitro* and *in vivo*.

Ethical statement

All animal procedures were performed in accordance with the Guidelines for Care and Use of Laboratory Animals of Guangdong Pharmaceutical University and experiments were approved by the Animal Ethics Committee of Guangdong Pharmaceutical University.

Conflicts of interest

The authors declare no competing financial interest.

Acknowledgements

This work was supported by the Science and Technology Planning Project of Guangzhou (No. 202002030089), the National Science Foundation of China (No. 21802026, 31971314), special funds of key disciplines construction from Guangdong and Zhongshan cooperating, the Distinguished Youth Foundation of Anhui Province (1808085J05), the Fundamental Research Funds for the Central Universities of China (Grant No. JZ2017HGPA0164).

References

1 X. Chen, Y. Zhou, X. Peng and J. Yoon, Fluorescent and colorimetric probes for detection of thiols, *Chem. Soc. Rev.*, 2010, **39**, 2120–2135.

2 H. S. Jung, X. Chen, J. S. Kim and J. Yoon, Recent progress in luminescent and colorimetric chemosensors for detection of thiols, *Chem. Soc. Rev.*, 2013, **42**, 6019–6031.
3 Z. Xu and L. Xu, Fluorescent probes for the selective detection of chemical species inside mitochondria, *Chem. Commun.*, 2016, **52**, 1094–1119.
4 K. P. Carter, A. M. Young and A. E. Palmer, Fluorescent sensors for measuring metal ions in living systems, *Chem. Rev.*, 2014, **114**, 4564–4601.
5 K. Y. Zhang, Q. Yu, H. J. Wei, S. J. Liu, Q. Zhao and W. Huang, Long-lived emissive probes for time-resolved photoluminescence bioimaging and biosensing, *Chem. Rev.*, 2018, **118**, 1770–1839.
6 L. Banci, I. Bertini, S. Ciofi-Baffoni, T. Kozyreva, K. Zovo and P. Paulmaa, Affinity gradients drive copper to cellular destinations, *Nature*, 2010, **465**, 645–648.
7 S. C. Dodani, S. C. Leary, P. A. Cobine, D. R. Winge and C. J. Chang, A targetable fluorescent sensor reveals that copper-deficient SCO1 and SCO2 patient cells prioritize mitochondrial copper homeostasis, *J. Am. Chem. Soc.*, 2011, **133**, 8606–8616.
8 J. H. Viles, Metal ions and amyloid fiber formation in neurodegenerative diseases. Copper, zinc and iron in Alzheimer's, Parkinson's and prion diseases, *Coord. Chem. Rev.*, 2012, **256**, 2271–2284.
9 R. Krame, Fluorescent chemosensors for Cu^{2+} ions: fast, selective, and highly sensitive, *Angew. Chem., Int. Ed.*, 1998, **37**, 772–773.
10 K. J. Barnham and A. I. Bush, Biological metals and metal-targeting compounds in major neurodegenerative diseases, *Chem. Soc. Rev.*, 2014, **43**, 6727–6749.
11 X. Zhang, J. Lu, X. Ren, Y. Du, Y. Zheng, P. V. Ioannou and A. Holmgren, Oxidation of structural cysteine residues in thioredoxin 1 by aromatic arsenicals enhances cancer cell cytotoxicity caused by the inhibition of thioredoxin reductase 1, *Free Radicals Biol. Med.*, 2015, **152**, 192–200.
12 H. Chen, Y. H. Tang, M. G. Ren and W. Y. Lin, Single near-infrared fluorescent probe with high- and low-sensitivity sites for sensing different concentration ranges of biological thiols with distinct modes of fluorescence signals, *Chem. Sci.*, 2016, **7**, 1896–1903.
13 N. Kaur, S. Chopra, G. Singh, P. Raj, A. Bhasin, S. K. Sahoo, A. Kuwar and N. Singh, Chemosensors for biogenic amines and biothiols, *J. Mater. Chem. B.*, 2018, **6**, 4872–4902.
14 Z. Lu, Y. Lu, C. Fan, X. Sun, M. Zhang and Y. Lu, A two-separated-emission fluorescent probe for simultaneous discrimination of Cys/Hcy and GSH upon excitation of two different wavelengths, *J. Mater. Chem. B.*, 2018, **6**, 8221–8227.
15 H. R. Lu, H. T. Zhang, J. Chen, J. C. Zhang, R. C. Liu, H. Y. Sun, Y. L. Zhao, Z. F. Chai and Y. Hu, A thiol fluorescent probe reveals the intricate modulation of cysteine's reactivity by Cu(II), *Talanta*, 2016, **146**, 477–482.
16 L. Wu, A. C. Sedgwick, X. Sun, S. D. Bull, X. P. He and T. D. James, Reaction-based fluorescent probes for the detection and imaging of reactive oxygen, nitrogen, and sulfur species, *Acc. Chem. Res.*, 2019, **52**, 2582–2597.
17 D. Wu, A. C. Sedgwick, T. Gunnlaugsson, E. U. Akkaya, J. Yoon and T. D. James, Fluorescent chemosensors: the past, present and future, *Chem. Soc. Rev.*, 2017, **46**, 7105–7123.
18 Y. Yue, F. Huo, F. Cheng, X. Zhu, T. Mafireyi, R. M. Strongin and C. Yin, Functional synthetic probes for selective targeting and multi-analyte detection and imaging, *Chem. Soc. Rev.*, 2019, **48**, 4155–4177.
19 X. Li, Y. Zheng, H. Tong, R. Qian, L. Zhou, G. Liu, Y. Tang, H. Li, K. Lou and W. Wang, Rational design of an ultrasensitive and highly selective chemodosimeter by a dual quenching mechanism for cysteine based on a facile nichael-transcyclization cascade reaction, *Chem.–Eur. J.*, 2016, **22**, 9247–9256.
20 C. Yang, X. Wang, L. Shen, W. Deng, H. Liu, S. Ge, M. Yan and X. Song, An aldehyde group-based P-acid probe for selective fluorescence turn-on sensing of cysteine and homocysteine, *Biosens. Bioelectron.*, 2016, **80**, 17–23.
21 Q. T. Meng, H. M. Jia, P. Succar, L. Zhao, R. Zhang, C. Y. Duan and Z. Q. Zhang, A highly selective and sensitive ON-OFF-ON fluorescence chemosensor for cysteine detection in endoplasmic reticulum, *Biosens. Bioelectron.*, 2015, **74**, 461–468.
22 P. Y. Zhang, Y. Wang, W. X. Huang, Z. Q. Zhao, H. H. Li, H. T. Wang, C. X. He, J. H. Liu and Q. L. Zhang, "Turn off-on" phosphorescent sensor for biothiols based on a Ru-Cu ensemble, *Sens. Actuators, B*, 2018, **255**, 283–289.
23 B. P. Guo, X. Z. Pan, Y. F. Liu, L. X. Nie, H. Z. Zhao and Y. Z. Liu, A reversible water-soluble naphthalimide-based chemosensor for imaging of cellular copper(II) ion and cysteine, *Sens. Actuators, B*, 2018, **256**, 632–638.
24 Y. Singh, S. Arun, B. K. Singh, P. K. Dutta and T. Ghosh, Colorimetric and ON-OFF-ON fluorescent chemosensor for the sequential detection of Cu(II) and cysteine and its application in imaging of living cells, *RSC Adv.*, 2016, **6**, 80268–80274.
25 W. Hao, A. McBride, S. McBride, J. P. Gao and Z. Y. Wang, Colorimetric and near-infrared fluorescence turn-on molecular probe for direct and highly selective detection of cysteine in human plasma, *J. Mater. Chem.*, 2011, **21**, 1040–1048.
26 Y. M. Yang, Q. Zhao, W. Feng and F. Y. Li, Luminescent chemodosimeters for bioimaging, *Chem. Rev.*, 2013, **113**, 192–270.
27 R. Zhang and J. L. Yuan, Responsive metal complex probes for time-gated luminescence biosensing and imaging, *Acc. Chem. Res.*, 2020, **53**, 1316–1329.
28 K. K. W. Lo, Luminescent Rhenium(I) and Iridium(III) polypyridine complexes as biological probes, imaging reagents, and photocytotoxicagents, *Acc. Chem. Res.*, 2015, **48**, 2985–2995.
29 D. L. Ma, S. Lin, W. H. Wang, C. Yang and C. H. Leung, Luminescent chemosensors by using cyclometalated iridium(III) complexes and their applications, *Chem. Sci.*, 2017, **8**, 878–889.
30 Y. You, Y. Han, Y. M. Lee, S. Y. Park, W. Nam and S. J. Lippard, Phosphorescent sensor for robust

quantification of copper(II) ion, *J. Am. Chem. Soc.*, 2011, **133**, 11488–11491.

31 Z. Mao, M. Wang, J. Liu, L. J. Liu, S. M. Y. Lee, C. H. Leung and D. L. Ma, A long lifetime switch-on iridium(III) chemosensor for the visualization of cysteine in live zebrafish, *Chem. Commun.*, 2016, **52**, 4450–4453.

32 Z. Du, R. Zhang, B. Song, W. Zhang, Y. L. Wang, J. Liu, C. Liu, Z. P. Xu and J. Yuan, Iridium(III) complex-based activatable probe for phosphorescent/time-gated luminescent sensing and imaging of cysteine in mitochondria of live cells and animals, *Chem.–Eur. J.*, 2019, **25**, 1498–1506.

33 W. J. Xu, X. Zhao, W. Lv, H. R. Yang, S. J. Liu, H. Liang, Z. Z. Tu, H. Xu, W. L. Qiao, Q. Zhao and W. Huang, Rational design of phosphorescent chemodosimeter for reaction-based one-and two-photon and time-resolved luminescent imaging of biothiols in living cells, *Adv. Healthcare Mater.*, 2014, **3**, 658–669.

34 A. Stephenson and M. D. Ward, An octanuclear coordination cage with a 'cuneane' core-a topological isomer of a cubic cage, *Dalton Trans.*, 2011, **40**, 7824–7826.

35 D. L. Ma, H. Z. He, K. H. Leung, D. S. H. Chan and C. H. Leung, Bioactive luminescent transition-metal complexes for biomedical applications, *Angew. Chem., Int. Ed.*, 2013, **52**, 7666–7682.

36 P. Y. Zhang, L. M. Pei, Y. Chen, W. C. Xu, Q. T. Lin, J. Q. Wang, J. H. Wu, Y. Shen, L. N. Ji and H. Chao, A dinuclear ruthenium(II) complex as a one-and two-photon luminescent probe for biological Cu^{2+} detection, *Chem.–Eur. J.*, 2013, **19**, 15494–15503.

37 X. J. Liu, N. Zhang, T. Bing and D. H. Shangguan, Carbon dots based dual-emission silica nanoparticles as a ratiometricnanosensor for Cu^{2+}, *Anal. Chem.*, 2014, **86**, 2289–2296.

38 L. Wang, X. Gong, Q. Bing and G. Wang, A new oxadiazole-based dual-mode chemosensor: colorimetric detection of Co^{2+} and fluorometric detection of Cu^{2+} with high selectivity and sensitivity, *Microchem. J.*, 2018, **142**, 279–287.

39 X. Zhou, X. Jin, G. Sun and X. Wu, A sensitive and selective fluorescent probe for cysteine based on a new response-assisted electrostatic attraction strategy: the role of spatial charge configuration, *Chem.–Eur. J.*, 2013, **19**, 7817–7824.

40 Y. T. Yang, Y. B. Li, X. M. Zhi, Y. J. Xu and M. N. Li, A red-emitting luminescent probe for sequentially detecting Cu^{2+} and cysteine/histidine in aqueous solution and its imaging application in living zebrafish, *Dyes Pigm.*, 2020, **183**, 108690.

41 L. Xu, Y. Xu, W. Zhu, B. Zeng, C. Yang, B. Wu and X. Qian, Versatile trifunctional chemosensor of rhodamine derivative for Zn^{2+}, Cu^{2+} and His/Cys in aqueous solution and living cells, *Org. Biomol. Chem.*, 2011, **9**, 8284–8287.

42 Y. S. Yuan, X. Zhao, S. P. Liu, Y. F. Li, Y. Shi, J. J. Yan and X. L. Hu, A fluorescence switch sensor used for D-Penicillamine sensing and logic gate based on the fluorescence recovery of carbon dots, *Sens. Actuators, B*, 2016, **236**, 565–573.

43 J. N. Demas and J. W. Addington, Luminescence quenching of dicyanobis (1,10-phenanthroline) ruthenium(II) by cupric ion in aqueous solutions. Dynamic and static processes, *J. Am. Chem. Soc.*, 1974, **96**, 3663–3664.